

---

# Harnessing spectral representations for subgraph alignment

---

**Marco Pegoraro**

Sapienza University of Rome

**Riccardo Marin**

Sapienza University of Rome

**Arianna Rampini**

Sapienza University of Rome

**Simone Melzi**

Bicocca University of Milan

**Luca Cosmo**

Ca' Foscari University of Venice

**Emanuele Rodolà**

Sapienza University of Rome

## Abstract

With the rise and advent of graph learning techniques, graph data has become ubiquitous. However, while several efforts are being devoted to the design of new convolutional architectures, pooling or positional encoding schemes, less effort is being spent on problems involving maps between (possibly very large) graphs, such as signal transfer, graph isomorphism and subgraph correspondence. With this paper, we anticipate the need for a convenient framework to deal with such problems, and focus in particular on the challenging subgraph alignment scenario. We claim that, first and foremost, the *representation* of a map plays a central role on how these problems should be modeled. Taking the hint from recent work in geometry processing, we propose the adoption of a spectral representation for maps that is compact, easy to compute, robust to topological changes, easy to plug into existing pipelines, and is especially effective for subgraph alignment problems. We report for the first time a surprising phenomenon where the partiality arising in the subgraph alignment task is manifested as a special structure of the map coefficients, even in the absence of exact subgraph isomorphism, and which is consistently observed over different families of graphs up to several thousand nodes.

## 1 Introduction

The ability to align data is at the heart of many successful techniques in machine learning and related areas. In its most abstract form, the problem has a straightforward formulation: Given two generic domains  $D_1$  and  $D_2$ , find a transformation  $T$  such that  $TD_1 \approx D_2$  according to some approximation metric that depends on the task. Examples of such problems are found in numerous applications, including molecular docking, image-based rendering, 3D reconstruction, generative models and style transfer, in addition to countless others. Recent remarkable examples include CLIP [33], where images are associated to corresponding captions by aligning their learned embeddings, or MaSIF [15], where the interaction site between protein structures (i.e., the surface patches where the proteins geometrically align) is predicted by a geometric deep learning pipeline.

Perhaps the most challenging setting for alignment problems arises whenever the two domains only correspond *partially*, for example due to the lack of observations or noise in the data. In this case, one is not only interested in aligning the two domains, but also in discovering which portions of the

domains actually align. The problem is particularly hard if an exact alignment does not even exist, requiring additional robustness to local perturbations in the data.

In this paper, we focus on the general problem of subgraph alignment, as it is representative of a broad spectrum of applications including those mentioned above. We assume to be given two graphs  $G_1$  and  $G_2$ , where  $G_2$  appears within  $G_1$ , possibly up to topological changes. A special case appears when  $G_2$  is isomorphic to a subgraph of  $G_1$ , which is referred to as subgraph isomorphism. This case is included in our treatment, but we also consider noisier settings where a subgraph isomorphism does not exist, yet a semantic correspondence can still be defined.

**Contribution.** We focus in particular on the choice of a *representation* for the correspondence. That is, instead of introducing a new matching pipeline to solve subgraph alignment, we show an alternative way of representing maps between a graph and its subgraphs. In cases where the map is unknown and must be sought for, the new representation makes the inference problem easier to solve; while if the map is given, the new representation is more compact, has a regularizing effect, and bears a natural structure that is missing from classical representations such as node-to-node binary correspondence matrices.

From a technical perspective, the map representation is defined with respect to a spectral basis; namely, the eigenvectors of the graph Laplacian. This idea, introduced a decade ago in the geometry processing area [37], brought significant progress to several tasks in graphics and vision – yet, its application to graphs has been largely overlooked.

We claim that part of the reason is a common misconception. The lack of a smooth metric (i.e., a smooth manifold underlying the graph) leads to the assumption that key properties of the spectral representation of the maps, such as those observed in [37, 43], only exist for surface domains. With this work, we challenge this view by showing extensive empirical evidence that not only these spectral maps are applicable to general subgraphs, but also that they exhibit robustness properties that go beyond what has been shown on surfaces. Therefore, we propose to embrace the spectral representation of maps as compact, efficient, interpretable, robust, and easy to manipulate objects that can be naturally integrated into several pipelines, including but not limited to graph learning models.

We summarize our main contributions as follows:

- We propose the adoption of spectral representations for maps between graphs and *subgraphs*. For the first time, we show that such maps exhibit a special structure in their coefficients, which captures the similarity between the Laplacian eigenspaces of the two graphs.
- We further show robustness of the representation to topological modifications of the subgraph, due for example to graph rewiring. This leads to well-defined maps even in the absence of exact isomorphism.
- We include extensive experiments showing practical applications on graphs spanning a few dozen to tens of thousands of nodes, and demonstrate key benefits in terms of robustness to noise, regularizing effect, interpretability, and computational complexity.

All the code and generated data will be publicly released upon acceptance.

## 2 Related work

Graph alignment problems are ubiquitous in applications from social network analysis [28] to bioinformatics [45]. Given its relevance, a rich body of literature is devoted to this problem. A comparative study on several network alignment techniques can be found in [46]. Though not exhaustive, we discuss the most relevant works in the following.

**Node-to-node correspondence.** Focusing on the problem of protein-to-protein interaction (PPI), IsoRank [45] leverages graph topology information. It constructs an eigenvalue problem for every pair of input networks and extracts a global alignment across a set of networks by a k-partite matching. It was improved in [26] by spectral clustering on the induced graph of pairwise alignment scores. Similarly, EigenAlign variants [13, 35] propose to compute the eigenvectors of a joint adjacency matrix between the two input graphs and solve for the correspondence modeled as an optimization problem. More recently, [24] aims at optimizing for a permutation matrix between social networks modeled as bipartite graphs. FINAL [52] defines three criteria to align two graphs which are structure

similarity, node feature similarity and edge feature similarity, thus considering both attribute and topology information.

Differently from the previous approaches, [21, 50] modeled the correspondence optimization process as a propagation of ground-truth matches over the two input graphs. Unfortunately, these methods require an input sparse correspondence between the graphs that in many cases is not available.

More similar to our approach, in [23] Laplacian eigenvectors are used as a low-dimensional node embedding of near-isometric input graph nodes, which are then treated as point clouds and rigidly aligned. Due to this constraint, the authors deal only with the problem of non-rigid isometric meshes. With the same idea of working on a node embedding space, REGAL [18] constructs node embeddings based on the connectivity structure and node attributes, and uses the similarity between these features for node alignment. CONE-Align [6] models intra-network proximity with node embeddings and uses them to match nodes across networks after aligning the embedding subspaces. IONE [28], PALE [30], and DeepLink [54] propose to use representation learning methods to achieve node embeddings better reflecting the similarity between corresponding entities in social networks, thus requiring manually corresponding matches during the training phase.

All these methods directly look for a node-wise correspondence between input graphs, becoming soon infeasible when the size of the graphs reaches thousands of nodes. We investigate a different approach, studying the adoption of a functional representation to define a correspondence between graphs. Furthermore, previous works mostly focus on a single application, either global PPI network alignment [26, 45], synthetic datasets with structural noise (where a small portion of edges is randomly removed) [19, 46], or social networks [28, 30, 54]. In our analysis, we address the general task of *subgraph alignment*, where a large portion of the graph is missing, without focusing on any specific domain. This is also different from the problem of subgraph *isomorphism*, which concerns the decision problem as to whether small query graphs exist within larger graphs [11].

**Functional correspondence.** The functional maps framework [37] was first introduced in the shape analysis field to find correspondences between deformable 3D shapes. Thanks to its flexibility, many extensions of this framework have been later proposed, allowing to increase the correspondence accuracy by requiring a specific structure of the functional map by means of dedicated regularizers [12, 34, 36, 38, 41]. To allow matching non-isometric shapes, the authors of [25] apply the framework to approximate eigenbases obtained with a joint diagonalization algorithm.

The same approach was later fruitfully adapted to *partial* shape matching, where the goal is to map a part of a deformed shape to a full model. Seminal works in this regard are partial functional maps [43] and fully spectral partial shape matching [27]. The framework was further extended in [9] to deal with clutter, leading to a functional representation for partial-to-partial shape matching.

In the context of graphs, a first attempt to represent similarity between graphs in a functional space was proposed in [47]. However, there the functional representation is on the edge domain, and its application is limited to the case of Euclidean graphs. More related to our work is the recent GRASP [19], which detects an alignment among graphs by employing a functional correspondence among pre-aligned Laplacian eigenvectors. Different to our work, GRASP considers only the setting of noisy complete graphs, i.e. the original network is perturbed by randomly deleting edges with a probability  $p$  up to 0.25. Instead, we study the functional representation of the correspondence on a much broader class of graphs, undergoing strong partiality transformations in addition to strong perturbation of the connectivity, and consider larger scales reaching up to several thousand nodes.

### 3 Background

**Graphs and Laplacian eigenvectors.** We consider undirected, unweighted graphs  $G_1 = (V_1, E_1)$  with nodes  $V_1$  and edges  $E_1 \subseteq V_1 \times V_1$ . We denote as  $A_1 \in \{0, 1\}^{|V_1| \times |V_1|}$  the adjacency matrix of  $G_1$ , which is a binary matrix where  $A_1(i, j) = 1$  if an edge connects node  $i$  to node  $j$ , and  $A_1(i, j) = 0$  otherwise.

The normalized graph Laplacian for  $G_1$  is defined as the square matrix  $\mathcal{L}_1 = I - D_1^{-\frac{1}{2}} A_1 D_1^{-\frac{1}{2}} \in \mathbb{R}^{|V_1| \times |V_1|}$ , where  $D_1$  is a diagonal matrix of node degrees, with entries  $D_1(i, i) = \sum_{j=1}^{|V_1|} A_1(i, j)$ . This linear operator is symmetric and positive semi-definite; it admits an eigendecomposition  $\mathcal{L}_1 = \Phi_1 \Lambda_1 \Phi_1^\top$ , where  $\Lambda_1$  is a diagonal matrix that contains the eigenvalues, and  $\Phi_1$  is a matrix having as

columns the corresponding eigenvectors. Throughout this paper, we assume the eigenvalues (and corresponding eigenvectors) to be sorted in non-descending order  $0 = \lambda_1 \leq \lambda_2 \leq \dots \leq 2$ ; this assumption is important for interpreting the functional maps that we define in the sequel.

Each eigenvector  $\phi_l$  for  $l = 1, \dots, |V_1|$  has length  $|V_1|$ , and can be interpreted as a scalar function defined on the nodes of the graph; for this reason, we will occasionally refer to them as *eigenfunctions* for added clarity. These eigenfunctions form an orthonormal basis for the space of functions defined on the graph nodes. Usually, one may consider a subset of eigenfunctions, namely those associated with the  $k$  smallest eigenvalues, to approximate the graph signals in a compact way.

**Subgraph alignment.** In this work, we consider subgraphs  $G_2 = (V_2, E_2)$  of  $G_1$ , such that  $V_2 \subseteq V_1$  and  $E_2 \subseteq E_1$ . As done for  $G_1$ , we define the adjacency matrix  $A_2$  and the Laplacian  $\mathcal{L}_2$ .

We focus on the *subgraph alignment* problem, that is classically defined as follows. For all  $q \in V_2$ , one seeks the most similar node  $p$  in  $V_1$  with respect to a similarity measure  $s(p, q) \in [0, 1]$ ; all the pairwise similarities are encoded in a matrix  $S \in \mathbb{R}^{|V_1| \times |V_2|}$ . In the special case where  $G_2$  is isomorphic to a subgraph of  $G_1$ , the matrix  $S$  consists of a permutation matrix, with additional empty rows associated to the points in  $G_1$  which do not have a correspondence in  $G_2$ ; the combinatorial problem of inferring such a matrix is NP-complete [7].

In the general case, the similarity matrix  $S$  does not have any special structure, and its size grows with the size of  $G_1$  and  $G_2$ . In the following we introduce an alternative representation that is independent of the size of the graphs, and that can be easily obtained by a change of basis of the matrix  $S$ .

**Functional maps.** Ours is a direct adaptation of the functional map representation introduced in [37] for pairs of quasi-isometric surfaces. We present the original framework for surfaces here, and discuss its application to graphs and subgraphs in Section 4.

Consider two smooth manifolds  $\mathcal{M}$  and  $\mathcal{N}$ , and let  $T : \mathcal{N} \rightarrow \mathcal{M}$  be a point-to-point map between them. Given a scalar function  $f : \mathcal{M} \rightarrow \mathbb{R}$ , the map  $T$  induces a functional mapping via the composition  $g = f \circ T$ , which can be seen as a linear map  $T_F : f \mapsto g$  from the space of functions on  $\mathcal{M}$  to the space of functions on  $\mathcal{N}$ . As a linear map, the functional  $T_F$  admits a matrix representation after choosing a basis for the two function spaces.

To this end, consider the first  $k$  eigenfunctions of the Laplace-Beltrami operators for  $\mathcal{M}$  and  $\mathcal{N}$ , encoded in the matrices  $\Phi$  and  $\Psi$  respectively. Further, assume the pointwise map  $T$  is available and encoded in a binary matrix  $S$ , such that  $S(y, x) = 1$  if  $y \in \mathcal{N}$  corresponds to  $x \in \mathcal{M}$ , and 0 otherwise. By choosing  $\Phi$  and  $\Psi$  as bases, the functional map  $T_F$  can be encoded in a small  $k \times k$  matrix  $C$  via the change of basis formula:

$$C = \Psi^\dagger S \Phi, \tag{1}$$

where  $\dagger$  is the Moore-Penrose pseudoinverse. The size of  $C$  does *not* depend on the number of points in  $\mathcal{M}$  and  $\mathcal{N}$ , but only on the number  $k$  of basis functions. In other words,  $C$  represents the linear transformation that maps the coefficients of any given function  $f : \mathcal{M} \rightarrow \mathbb{R}$  expressed in the eigenbasis  $\Phi$ , to coefficients of a corresponding function  $g : \mathcal{N} \rightarrow \mathbb{R}$  expressed in the eigenbasis  $\Psi$ .

When the pointwise similarity  $S$  is unknown, one can directly compute the matrix  $C$  as the solution of a regularized least-squares problem with  $k^2$  unknowns, given some input features on the two surfaces (e.g., landmark matches or local descriptors). For further details we refer to [37, 38].

## 4 Functional maps for subgraphs

### 4.1 Motivation

As we have mentioned in Section 3, the classical way to represent a map as a similarity matrix  $S \in \mathbb{R}^{|V_1| \times |V_2|}$  is sub-optimal, because such matrices can be extremely sparse (especially in case of strong partiality), and their dimensions scale quadratically with the number of nodes in the graphs.

One can directly adapt Equation (1) to the case of graphs by replacing  $\Phi, \Psi$  with the eigenvectors of the normalized graph Laplacians, and therefore shift to a spectral representation of the map. However, recall that we consider the setting where  $G_2$  is a *subgraph* of  $G_1$ . This simple fact leads to the following important observation, that is central to our contribution:

In many practical cases, the eigenspaces of the normalized graph Laplacian are well preserved under *non-isomorphic* transformations of the graph, including strong partiality, topological perturbations, and edge rewiring.

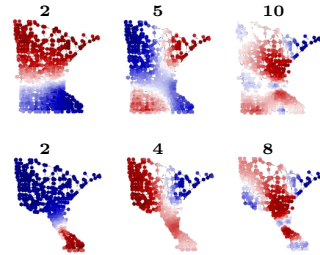
Put simply, the values of the Laplacian eigenfunctions stay approximately the same (up to sign, in case of simple spectrum) at the nodes that are not directly involved in the perturbation – which is to say that the eigenvectors of the partial graph  $G_2$ , encoded in  $\Psi$ , correlate strongly with the those of  $G_1$ , encoded in  $\Phi$ . This observation is not trivial and has not been reported before, to the best of our knowledge.

In the sequel we show extensive empirical evidence of this surprising behavior, and describe its practical consequences.

## 4.2 Map structure

To get a better understanding of this phenomenon, in the inset we show an example where the Laplacian eigenfunctions of a subgraph of the Minnesota graph (bottom row) strongly correlate with the eigenfunctions of the complete graph (top row), i.e., the Laplacian eigenfunctions have similar values at corresponding nodes, up to sign. Above each image, we also report the index of the plotted eigenfunction, leading to the following remark:

**Remark (eigenvector indexing):** The eigenfunctions of the complete graph and those of the subgraph do not necessarily correlate at the same index.



In the 3D geometry processing literature, a similar behavior was observed for the discrete Laplace-Beltrami operator under partiality transformations of smooth surfaces [40, 43]; however, the theoretical analysis presented in these works assumes to be given Riemannian surfaces with a smooth metric – an assumption that does *not* hold in the case of general graphs<sup>1</sup>

The most direct consequence of this preservation of eigenspaces is reflected in the structure of the functional map  $C$  that encodes the correspondence, computed via Equation (1). In Figure 1 we show this matrix when  $G_1$  is a graph shaped like a cat, and  $G_2, \dots$  are subgraphs at increasing levels of partiality; each subgraph is obtained by randomly removing up to 80% of the edges of  $G_1$ .

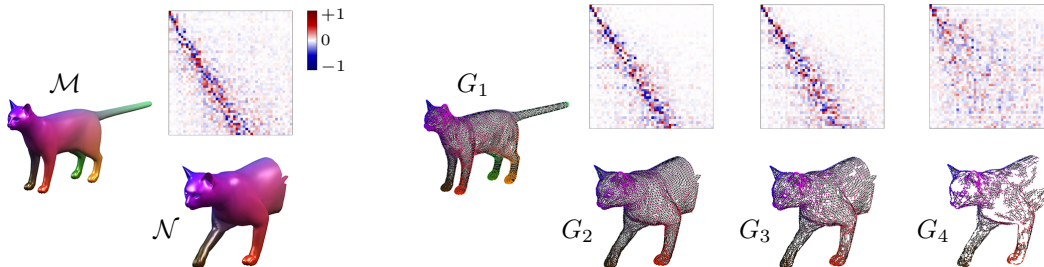


Figure 1: *Left:* Functional map matrix between a smooth surface  $\mathcal{M}$  and a deformed part  $\mathcal{N}$ ; the slanted-diagonal structure suggests that the eigenspaces of  $\mathcal{M}$  are mostly preserved in  $\mathcal{N}$ . *Right:* Functional map matrices between a graph  $G_1$  and the subgraphs  $G_2, G_3, G_4$ , obtained by removing 40%, 55%, and 80% of the edges from  $G_1$  respectively. The slanted-diagonal structure can still be observed, and gets dispersed only at very high partiality. In the graphs above, corresponding nodes have the same color.

In the experiment of Figure 1, the slanted-diagonal structure of the map between  $\mathcal{M}$  and  $\mathcal{N}$  is explained by an application of Weyl’s law to 2-dimensional Riemannian manifolds, see [43, Eq. 9]. However, there is no theoretical counterpart to explain the map structure between  $G_1$  and its subgraphs, due to the complete absence of metric information about the underlying surface: The

<sup>1</sup>From a numerical perspective, the main difference lies in how the Laplacian operator is discretized. For 3D meshes, a typical discretization (the so called ‘cotan Laplacian’ [39]) yields a matrix with continuous values depending on the angles between edges and the local areas computed on the surface. To the contrary, the normalized graph Laplacian does not even encode edge lengths, as it is purely based on graph connectivity.

eigenfunctions are computed *purely* from the graph connectivity. Yet, the diagonal structure is preserved even under rather dense removal of edges, suggesting deeper algebraic implications.

One might legitimately ask whether the presence of a structure in the maps of Figure 1 is due to the specific choice of the data, where the subgraphs derive from a 3D mesh (although the normalized graph Laplacian dismisses any edge length information) and where the type of partiality resembles a neat ‘cut’ (although we also perform random edge removals). However, the same behavior is observed in more generic and abstract cases, as we show in Figure 2 and in several other examples throughout the paper. The maps still show a clear structure, although the CORA graph does not have a natural geometric embedding.

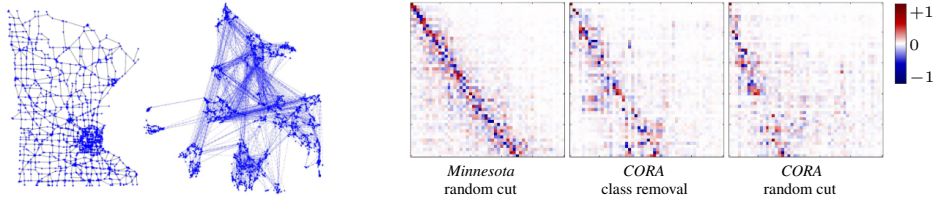


Figure 2: Functional maps between the Minnesota and CORA graphs (shown on the left) and their subgraphs. The subgraphs are obtained via random cuts or by entirely removing one random class; see captions below each matrix. Each subgraph only has 60% of the original nodes.

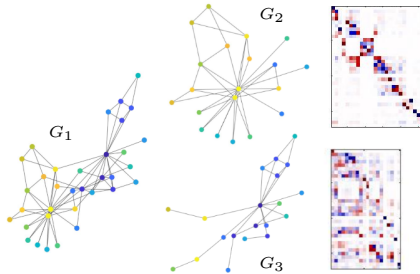
As we will show in Section 5, the presence of a sparse structure in the functional map matrix  $C$  can be directly used as a regularizer, in all those cases where the map is not given but must be estimated from the graph data.

### 4.3 Robustness to graph rewiring

To this point, we have considered cases where there exists an *exact* subgraph isomorphism between  $G_2$  and  $G_1$ , meaning that the subgraph  $G_2$  is fully contained in the bigger graph  $G_1$ . However, in many practical settings this might not be the case. In this Section we show that the spectral representation of the map is robust to local topological changes of the graph; in the graph learning literature, such perturbations frequently occur due to noise in the data, or are explicitly obtained by rewiring operations [5] or adversarial attacks [20] among others.

In our setting, for a map representation to be robust, we expect that small changes in graph connectivity lead to small changes in the matrix coefficients. We refer to Section 5 for extensive experiments on multiple datasets demonstrating this robustness.

Here we provide one qualitative example in the inset figure, where we show an experiment on the Karate dataset [51]. Given the complete graph  $G_1$ , we compare the functional map matrices corresponding to an exact, clean subgraph  $G_2$  (top row), and to a noisier subgraph  $G_3$  that further underwent a random local rewiring of its edges (bottom row). From this experiment, we make two key observations:



**Remark (map structure):** The functional map matrices are not necessarily diagonal, but may present a different sparsity structure which depends on the particular subgraph.

**Remark (topological changes):** The harder case, where there is partiality *in conjunction with* topological changes, still manifests a sparse structure in the coefficient matrix. More examples of this are shown below.

Both points above directly depend on graph connectivity, and it is hard to find analogies for smooth surfaces. We conjecture that local topological transformations of a graph, while they can certainly induce strong transformations of *some* of its Laplacian eigenspaces (similar to single-point perturbations on planar manifolds, see [14]), are less likely to distort *all* the eigenspaces at once. This way, the functional map matrix tends to maintain its global structure intact, and exhibits local perturbations.

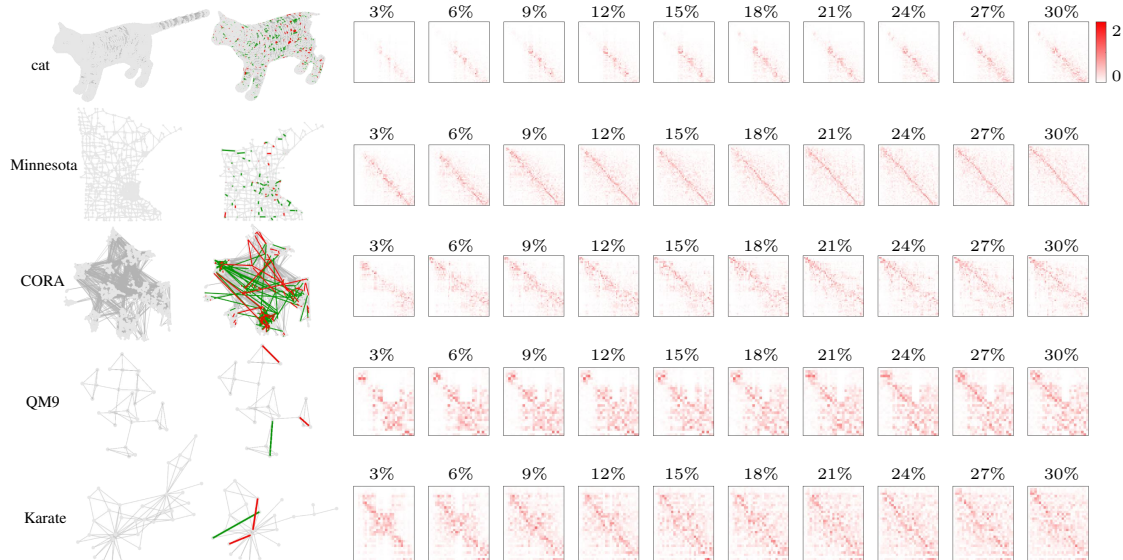


Figure 3: Robustness of the map to the simultaneous action of partiality and rewiring of the subgraph. The rewiring operations are increasingly stronger, with increments of 3% of the total number of edges (starting from 3% and reaching 30%). The plotted matrices encode the element-wise error of the functional map after the topological perturbations. Error is encoded as color, growing from white to red.

## 5 Theoretical results and analysis

In this section we validate the claims made in the previous sections with additional qualitative and numerical results. More experiments and details about the used datasets can be found in the **Supplementary Material**.

### 5.1 Robustness to rewiring

In section 4.3, we claimed that the functional representation is robust to changes in graph connectivity. In Figure 3, we test this behavior on different graphs. In each row, we select a graph  $G_1$  (pictured in the first column) and compute a subgraph  $G_2$  from it (second column). Then, we apply small incremental changes to the topology of the subgraph, with increments of 3% of the total number of edges; the changes are performed by removing and adding random edges, obtaining new sub graphs  $G_i$ . In the figure, in the second column we plot one representative example (per dataset) of such topological modifications, depicting the added edges in green, and the removed edges in red. The matrices appearing in the figure show the element-wise perturbation of the functional map matrix between  $G_1$  and  $G_2$  after performing the rewiring operations.

### 5.2 Signal transfer

Table 1: Normalized Mean Squared Error (MSE) obtained by transferring node features using the functional map on a truncated eigenbasis (50 eigenfunctions).

Dataset	Task	#nodes	Type	Subgraph	Features	MSE(%)
Citeseer [16]	classification	2120	citation	class	continuous and sparse	$0.0 \pm 0.0$
PubMed [44]	classification	19717	citation	class	continuous and sparse	$0.0 \pm 0.0$
PPI [17] 0	classification	1546	molecular	label	continuous	$2 \pm 0.0$
PPI [17] 13	classification	3480	molecular	label	continuous	$2 \pm 0.0$
FraudAmazon [53]	fraud detection	11944	reviews	edge type	mixed	$11 \pm 2$
Amazon Photo [31]	classification	7487	co-purchase	class	discrete and sparse	$18 \pm 2$
Amazon Computer [31]	classification	13381	co-purchase	class	discrete and sparse	$21 \pm 2$

Within a graph, nodes may often come with numerical or vector-valued attributes, encoding for instance molecular properties in PPIs, user identities in social networks, or positional encodings to

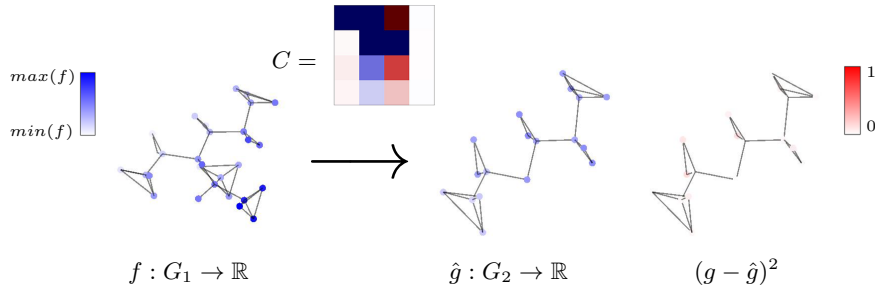


Figure 4: Illustrative example of a signal transferred from the graph  $G_1$  (left) to the sub-graph  $G_2$  (right) using the functional map matrix  $C$  (top). The rightmost graph reports the node-wise squared difference between the original and the reconstructed signal.

better distinguish and characterize nodes. Such data can be modeled as functions  $f : G_1 \rightarrow \mathbb{R}$  that map each node of  $G_1$  to a real value. The functional map  $C$  allows to transfer this function from a graph  $G_1$  to some subgraph  $G_2$  without requiring the computation of an explicit node-to-node correspondence.

In fact, it is sufficient to project the given  $f$  onto the Laplacian eigenfunctions of  $G_1$ , apply the linear transformation  $C$  to the obtained coefficients, and finally reconstruct the signal on the target graph  $G_2$  with respect to its Laplacian eigenfunctions. The described procedure is simply implemented by the formula:

$$\hat{g} = \Phi_2 C \Phi_1^\top f. \quad (2)$$

In Figure 4 we leverage this property of the spectral representation to transfer a signal defined on a graph to an example subgraph. Given a signal  $f$  defined over  $G_1$  (left), we transfer  $f$  to the subgraph  $G_2$  (middle) through the functional map  $C$  (top), obtaining a new signal  $\hat{g} : G_2 \rightarrow \mathbb{R}$ . To evaluate the fidelity of the transferred signal, we compute the mean squared error between the transferred signal  $\hat{g}$  and the ground truth signal  $g$  (obtained via the ground truth node-to-node correspondence) through the formula:  $\frac{\sum_{i=1}^n (\hat{g}_i - g_i)^2}{n(\max(f) - \min(f))^2}$ . In Table 1, we report a similar experiment on graphs from different datasets. We consider pairs composed by the original graph and a series of subgraphs extracted according to a semantic criterion, e.g., nodes belonging to the same class or nodes connected by the same type of edge. On each pair we transfer the signal defined over the original graph to the subgraph using a functional map represented in the first 50 eigenfunctions. The last column reports the average reconstruction error.

### 5.3 Node-to-node correspondence

Table 2: Comparison of the Mean Average Precision of the correspondence computed on different graphs by different methods.

	Partiality	IsoRank	FINAL	REGAL	PALE	GRASP	$FM_W$	$FM_W + ZM$	$GT$
Cat[10]		$0.1 \pm 0.0$	$0.2 \pm 0.0$	<b><math>93 \pm 1.9</math></b>	$6.8 \pm 0.4$	$11 \pm 0.0$	$68 \pm 14$	$69 \pm 14$	$92 \pm 3.9$
Minnesota	patch	$0.2 \pm 0.1$	$1 \pm 0.0$	$87 \pm 3.3$	$13 \pm 0.4$	$18 \pm 2$	$88 \pm 4$	$89 \pm 3.7$	<b><math>94 \pm 1.6</math></b>
Cora[32]		$0.5 \pm 0.0$	$0.6 \pm 0.0$	$54 \pm 3.5$	$22 \pm 2.9$	$6.8 \pm 1.8$	$33 \pm 9.4$	$34 \pm 9.5$	<b><math>65 \pm 3.1</math></b>
Cora[32]	class	$0.4 \pm 0.0$	$0.4 \pm 0.0$	$55 \pm 3.4$	$17 \pm 2$	$51 \pm 22$	$71 \pm 16$	$60 \pm 21$	<b><math>85 \pm 6.5</math></b>
Douban[49]	online-offline	0.6	1.1	<b>70</b>	6	0.7	0.8	0.8	3.1

One of the advantages of the spectral representation is to reduce the NP-hard problem of finding node-to-node correspondences (usually formulated as a quadratic assignment problem [29]) to the more tractable (polynomial) problem of finding the linear transformation between the reduced eigenbases of the graphs (at least under the reasonable assumption of smoothness of the sought correspondence, i.e., nearby nodes on the input graph are located nearby also on the target subgraph).

With this experiment we apply two functional map-based matching algorithms to recover such linear transformation and finally convert it to a node-to-node correspondence between the two input graphs. Specifically, we adopt the off-the-shelf partial functional map algorithm ( $FM_W$ ) [43] and then refine the correspondence with ZoomOut [34] ( $FM_W + ZM$ ). We compare the spectral representation with the network alignment methods proposed in the benchmark [46]: IsoRank [45], FINAL [52], REGAL [18] and PALE [30]. For all the methods, we use as input 50 landmark matches. For the



two functional map methods we truncate the eigenbasis to the first 50 eigenvectors and use smooth indicator functions computed on the given landmarks as corresponding functions. We refer to the supplementary material for further implementation details.

To investigate the degradation of the correspondence induced by the truncated eigenbasis, excluding errors generated by the matching algorithm, we also compute the correspondence starting from the ground-truth functional map (GT in the table).

We report in Table 2 the Mean Average Precision (MAP) defined as  $\frac{1}{n} \sum_{i=1}^n \frac{1}{ra_i}$  where  $ra_i$  is the rank (position) of positive matching node in the sequence of sorted candidates. For our evaluation we consider different graphs and subgraphs. The Cat graph is derived from the corresponding mesh of the Shrech2016 Partial Deformable Shapes benchmark [8]. We extract 10 partial graphs by considering k-hops subgraphs starting from random points. We perform a similar extraction also on Minnesota and CORA. As we can see from the *GT* column, the functional representation seems to preserve well the correspondence on these graphs, reaching the highest performance in almost all cases. Also the performance of the functional map based methods is satisfactory, being the best performing method in Minnesota and the second best in the other two datasets. The functional map seems to perform particularly well on the Minnesota graph. This is probably because it represents an example of planar graph, where an almost regular structure can be defined. On the other hand, social graphs like CORA, are characterized by a more irregular structure and few nodes with high degrees, which breaks the smoothness assumption of the truncated functional representation. The performance on CORA improves when the subgraph is semantically meaningful, obtained by removing all the nodes belonging to a specific class (fourth row).

Finally, we test the functional representation on Douban [49], a real-world dataset composed of an online and offline version of the same social network. In this case, both the nodes and connectivity are very different between the two graphs, resulting in incompatible eigenbases making this scenario particularly challenging for a functional representation, as can also be observed by the low accuracy achieved using the *GT* functional map.

## 6 Conclusions

The spectral representation of functional maps for encoding graph and subgraph correspondences lends itself well to several applications, and we anticipate that it will be a useful addition to the graph learning toolset. Among the promising directions that we aim to explore are the definition of novel positional encodings for graphs that are robust to partiality transformations and to graph rewiring, and the application of functional mapping to more abstract structures such as learned graph embeddings.

Further, while in this paper we showed extensive evidence that the spectral map representation bears a special structure depending on the type of partiality, currently we have not taken full advantage of this structure. When the task at hand requires seeking for the subgraph alignment, i.e. whenever the map is unknown, it may be possible to design stronger regularizers to induce sparsity in the matrix representation of the map. This is quite different from the better known setting of 3D surfaces, where this sparse structure is typically just diagonal or slanted-diagonal.

In the light of the increasing interest of the graph learning community toward spectral techniques, adopting a spectral representation for maps between graphs is a natural next step; it is simple to adopt, easy to manipulate, and memory-efficient, and has the potential to become a fundamental ingredient in spectral graph learning pipelines in the near future.

**Acknowledgements** This work is supported by the ERC Starting Grant No. 802554 (SPECGEO) and the SAPIENZA BE-FOR-ERC 2020 Grant (NONLINFMAPS).

## References

- [1] Yonathan Aflalo, Haim Brezis, and Ron Kimmel. On the optimality of shape and data representation in the spectral domain. *SIAM Journal on Imaging Sciences*, 8(2):1141–1160, 2015.
- [2] Mikhail Belkin and Partha Niyogi. Convergence of laplacian eigenmaps. In *Proc. NIPS*, pages 129–136, 2006.
- [3] P. J. Besl and N. D. McKay. A method for registration of 3-d shapes. *IEEE Transactions on Pattern Analysis and Machine Intelligence*, 14(2):239–256, Feb 1992.

- [4] Nicolas Boumal, Bamdev Mishra, Pierre-Antoine Absil, and Rodolphe Sepulchre. Manopt, a matlab toolbox for optimization on manifolds. *CoRR*, abs/1308.5200, 2013.
- [5] Benjamin Chamberlain, James Rowbottom, Davide Eynard, Francesco Di Giovanni, Xiaowen Dong, and Michael Bronstein. Beltrami flow and neural diffusion on graphs. In M. Ranzato, A. Beygelzimer, Y. Dauphin, P.S. Liang, and J. Wortman Vaughan, editors, *Advances in Neural Information Processing Systems*, volume 34, pages 1594–1609. Curran Associates, Inc., 2021.
- [6] Xiyuan Chen, Mark Heimann, Fatemeh Vahedian, and Danai Koutra. Cone-align: Consistent network alignment with proximity-preserving node embedding. In *Proceedings of the 29th ACM International Conference on Information & Knowledge Management*, pages 1985–1988, 2020.
- [7] Stephen A. Cook. The complexity of theorem-proving procedures. In *Proceedings of the Third Annual ACM Symposium on Theory of Computing*, STOC '71, page 151–158, New York, NY, USA, 1971. Association for Computing Machinery.
- [8] Luca Cosmo, Emanuele Rodola, Michael M Bronstein, Andrea Torsello, Daniel Cremers, and Y Sahillioglu. Shrec'16: Partial matching of deformable shapes. *Proc. 3DOR*, 2(9):12, 2016.
- [9] Luca Cosmo, Emanuele Rodolà, Jonathan Masci, Andrea Torsello, and Michael M Bronstein. Matching deformable objects in clutter. In *International Conference on 3D Vision (3DV)*, pages 1–10. IEEE, 2016.
- [10] L. Cosmo, E. Rodolà, M. M. Bronstein, A. Torsello, D. Cremers, and Y. Sahillioglu. Partial Matching of Deformable Shapes. In A. Ferreira, A. Giachetti, and D. Giorgi, editors, *Eurographics Workshop on 3D Object Retrieval*. The Eurographics Association, 2016.
- [11] Chi Thang Duong, Trung Dung Hoang, Hongzhi Yin, Matthias Weidlich, Quoc Viet Hung Nguyen, and Karl Aberer. Efficient streaming subgraph isomorphism with graph neural networks. *Proceedings of the VLDB Endowment*, 14(5):730–742, 2021.
- [12] Danielle Ezuz and Mirela Ben-Chen. Deblurring and denoising of maps between shapes. *Computer Graphics Forum*, 36(5):165–174, 2017.
- [13] Soheil Feizi, Gerald Quon, Mariana Recamonde-Mendoza, Muriel Medard, Manolis Kellis, and Ali Jadbabaie. Spectral alignment of graphs. *IEEE Transactions on Network Science and Engineering*, 7(3):1182–1197, 2019.
- [14] Marcel Filoche and Svitlana Mayboroda. Universal mechanism for anderson and weak localization. *Proceedings of the National Academy of Sciences*, 109(37):14761–14766, 2012.
- [15] Pablo Gainza, Freyr Sverrisson, Frederico Monti, Emanuele Rodola, D Boscaini, MM Bronstein, and BE Correia. Deciphering interaction fingerprints from protein molecular surfaces using geometric deep learning. *Nature Methods*, 17(2):184–192, 2020.
- [16] C. Lee Giles, Kurt D. Bollacker, and Steve Lawrence. Citeseer: An automatic citation indexing system. Association for Computing Machinery, 1998.
- [17] William L. Hamilton, Rex Ying, and Jure Leskovec. Inductive representation learning on large graphs. *CoRR*, abs/1706.02216, 2017.
- [18] Mark Heimann, Haoming Shen, Tara Safavi, and Danai Koutra. Regal: Representation learning-based graph alignment. In *Proceedings of the 27th ACM international conference on information and knowledge management*, pages 117–126, 2018.
- [19] Judith Hermanns, Anton Tsitsulin, Marina Munkhoeva, Alex Bronstein, Davide Mottin, and Panagiotis Karras. Grasp: Graph alignment through spectral signatures. In *Asia-Pacific Web (APWeb) and Web-Age Information Management (WAIM) Joint International Conference on Web and Big Data*, pages 44–52. Springer, 2021.
- [20] Wei Jin, Yaxing Li, Han Xu, Yiqi Wang, Shuiwang Ji, Charu Aggarwal, and Jiliang Tang. Adversarial attacks and defenses on graphs. *SIGKDD Explor. Newsl.*, 22(2):19–34, jan 2021.
- [21] Ehsan Kazemi, S Hamed Hassani, and Matthias Grossglauser. Growing a graph matching from a handful of seeds. *Proceedings of the VLDB Endowment*, 8(10):1010–1021, 2015.
- [22] Johannes Klicpera, Janek Groß, and Stephan Günnemann. Directional message passing for molecular graphs. *CoRR*, abs/2003.03123, 2020.
- [23] David Knossow, Avinash Sharma, Diana Mateus, and Radu Horaud. Inexact matching of large and sparse graphs using laplacian eigenvectors. In *International workshop on graph-based representations in pattern recognition*, pages 144–153. Springer, 2009.
- [24] Danai Koutra, Hanghang Tong, and David Lubensky. Big-align: Fast bipartite graph alignment. In *2013 IEEE 13th international conference on data mining*, pages 389–398. IEEE, 2013.
- [25] Artiom Kovnatsky, Michael M Bronstein, Alexander M Bronstein, Klaus Glashoff, and Ron Kimmel. Coupled quasi-harmonic bases. *Computer Graphics Forum*, 32(2pt4):439–448, 2013.
- [26] Chung-Shou Liao, Kanghao Lu, Michael Baym, Rohit Singh, and Bonnie Berger. Isorankn: spectral methods for global alignment of multiple protein networks. *Bioinformatics*, 25(12):i253–i258, 2009.

- [27] O. Litany, E. Rodolà, A. M. Bronstein, and M. M. Bronstein. Fully spectral partial shape matching. *Computer Graphics Forum*, 36(2):247–258, 2017.
- [28] Li Liu, William K Cheung, Xin Li, and Lejian Liao. Aligning users across social networks using network embedding. In *Ijcai*, pages 1774–1780, 2016.
- [29] Eliane Maria Loiola, Nair Maria Maia de Abreu, Paulo Oswaldo Boaventura Netto, Peter Hahn, and Tania Maia Querido. A survey for the quadratic assignment problem. *Eur. J. Oper. Res.*, 176(2):657–690, 2007.
- [30] Tong Man, Huawei Shen, Shenghua Liu, Xiaolong Jin, and Xueqi Cheng. Predict anchor links across social networks via an embedding approach. In *Ijcai*, volume 16, pages 1823–1829, 2016.
- [31] Julian J. McAuley, Christopher Targett, Qinfeng Shi, and Anton van den Hengel. Image-based recommendations on styles and substitutes. *CoRR*, abs/1506.04757, 2015.
- [32] Andrew McCallum, Kamal Nigam, and Jason Rennie. Automating the construction of internet portals. 2000.
- [33] Marina Meila and Tong Zhang, editors. *Proceedings of the 38th International Conference on Machine Learning, ICML 2021, 18-24 July 2021, Virtual Event*, volume 139 of *Proceedings of Machine Learning Research*. PMLR, 2021.
- [34] Simone Melzi, Jing Ren, Emanuele Rodolà, Abhishek Sharma, Peter Wonka, and Maks Ovsjanikov. Zoomout: Spectral upsampling for efficient shape correspondence. *ACM Transactions on Graphics (TOG)*, 38(6):155, 2019.
- [35] Huda Nassar, Nate Veldt, Shahin Mohammadi, Ananth Grama, and David F Gleich. Low rank spectral network alignment. In *Proceedings of the 2018 World Wide Web Conference*, pages 619–628, 2018.
- [36] Dorian Nogneng and Maks Ovsjanikov. Informative descriptor preservation via commutativity for shape matching. *Computer Graphics Forum*, 36(2):259–267, 2017.
- [37] Maks Ovsjanikov, Mirela Ben-Chen, Justin Solomon, Adrian Butscher, and Leonidas Guibas. Functional maps: a flexible representation of maps between shapes. *ACM Transactions on Graphics (TOG)*, 31(4):30:1–30:11, 2012.
- [38] Maks Ovsjanikov, Etienne Corman, Michael Bronstein, Emanuele Rodolà, Mirela Ben-Chen, Leonidas Guibas, Frederic Chazal, and Alex Bronstein. Computing and processing correspondences with functional maps. In *SIGGRAPH 2017 Courses*. 2017.
- [39] Ulrich Pinkall and Konrad Polthier. Computing discrete minimal surfaces and their conjugates. *Experimental mathematics*, 2(1):15–36, 1993.
- [40] E. Postolache, M. Fumero, L. Cosmo, and E. Rodolà. A parametric analysis of discrete hamiltonian functional maps. *Computer Graphics Forum*, 39(5):103–118, 2020.
- [41] Jing Ren, Simone Melzi, Maks Ovsjanikov, and Peter Wonka. Maptree: Recovering multiple solutions in the space of maps. *ACM Trans. Graph.*, 39(6), Nov. 2020.
- [42] Jing Ren, Mikhail Panine, Peter Wonka, and Maks Ovsjanikov. Structured regularization of functional map computations. *CoRR*, abs/2009.14624, 2020.
- [43] Emanuele Rodolà, Luca Cosmo, Michael M Bronstein, Andrea Torsello, and Daniel Cremers. Partial functional correspondence. *Computer Graphics Forum*, 36(1):222–236, 2017.
- [44] Prithviraj Sen, Galileo Namata, Mustafa Bilgic, Lise Getoor, Brian Galligher, and Tina Eliassi-Rad. Collective classification in network data. *AI Magazine*, 29(3):93, Sep. 2008.
- [45] Rohit Singh, Jinbo Xu, and Bonnie Berger. Global alignment of multiple protein interaction networks with application to functional orthology detection. *Proceedings of the National Academy of Sciences*, 105(35):12763–12768, 2008.
- [46] Huynh Thanh Trung, Nguyen Thanh Toan, Tong Van Vinh, Hoang Thanh Dat, Duong Chi Thang, Nguyen Quoc Viet Hung, and Abdul Sattar. A comparative study on network alignment techniques. *Expert Systems with Applications*, 140:112883, 2020.
- [47] Fu-Dong Wang, Nan Xue, Yipeng Zhang, Gui-Song Xia, and Marcello Pelillo. A functional representation for graph matching. *IEEE transactions on pattern analysis and machine intelligence*, 2019.
- [48] H. Weyl. Ueber die asymptotische verteilung der eigenwerte. *Nachrichten von der Gesellschaft der Wissenschaften zu Göttingen, Mathematisch-Physikalische Klasse*, 1911:110–117, 1911.
- [49] Yu Wu, Wei Wu, Ming Zhou, and Zhoujun Li. Sequential match network: A new architecture for multi-turn response selection in retrieval-based chatbots. *CoRR*, abs/1612.01627, 2016.
- [50] Lyudmila Yartseva and Matthias Grossglauser. On the performance of percolation graph matching. In *Proceedings of the first ACM conference on Online social networks*, pages 119–130, 2013.
- [51] Wayne W. Zachary. An information flow model for conflict and fission in small groups. *Journal of Anthropological Research*, 33(4):452–473, 1977.

- [52] Si Zhang and Hanghang Tong. Final: Fast attributed network alignment. In *Proceedings of the 22nd ACM SIGKDD international conference on knowledge discovery and data mining*, pages 1345–1354, 2016.
- [53] Shijie Zhang, Hongzhi Yin, Tong Chen, Quoc Viet Hung Nguyen, Zi Huang, and Lizhen Cui. Gcn-based user representation learning for unifying robust recommendation and fraudster detection. *CoRR*, abs/2005.10150, 2020.
- [54] Fan Zhou, Lei Liu, Kunpeng Zhang, Goce Trajcevski, Jin Wu, and Ting Zhong. Deeplink: A deep learning approach for user identity linkage. In *IEEE INFOCOM 2018-IEEE conference on computer communications*, pages 1313–1321. IEEE, 2018.

# Supplementary Material

## A Interpretation of the functional map matrix

### A.1 Matrix representation

In the case of graphs, the functional map matrix is simply written as:

$$C = \Psi^\top S \Phi, \quad (3)$$

where  $\Phi, \Psi$  contain the eigenvectors of the normalized graph Laplacians of  $G_1$  and  $G_2$  respectively, and  $S$  is a matrix encoding the node-to-node correspondence. Note that differently from the case of surface meshes, in Equation 3 we write  $\Psi^\top$  instead of using the pseudo-inverse  $\Psi^\dagger$ ; this is due to the fact that the graph Laplacian eigenvectors are orthogonal with respect to the standard dot product, i.e.,  $\Psi^\top \Psi = I$  and  $\Phi^\top \Phi = I$ . This makes the matrix  $C$  easy to compute by simple matrix multiplication.

### A.2 Interpretation of the structure of $C$

One important property of the map representation  $C$  is its interpretability as a matrix of dot products. According to Equation 3, each coefficient  $c_{ij}$  of  $C$  corresponds to an inner product between  $\psi_i$  and  $S\phi_j$ . Therefore, each such inner product measures the correlation *at corresponding nodes* between a Laplacian eigenvector  $\psi_i$  of  $G_2$ , and a Laplacian eigenvector  $\phi_j$  of  $G_1$ . Another way to see this is as follows: each eigenvector  $\psi_i$  is expressed as a linear combination of eigenvectors  $S\phi_j$ , and the combination coefficients are stored in row  $i$  of  $C$ .

Based on experimental evidence, we distinguish among the following three cases; recall that we assume the eigenvectors of the two graphs to be ordered by increasing eigenvalue. We refer to Figure 5 for a visual reference.

- **(i) Isomorphic graphs.** The two graphs have exactly the same eigenspaces. Thus, matrix  $C$  is diagonal with  $\pm 1$  along the diagonal, because  $c_{ij} = 0$  for  $i \neq j$  (due to orthogonality of the eigenvectors), while  $c_{ii} = \pm 1$  (due to the sign ambiguity of the eigenvectors). In case of repeated eigenvalues, one may observe small blocks of coefficients along the diagonal due to the non-uniqueness on the choice of the eigenvectors spanning high-dimensional eigenspaces.
- **(ii) Isomorphic subgraphs (this paper).** The two graphs have partially similar eigenspaces, meaning that the inner products between  $\psi_i$  and  $S\phi_j$  tend to be close to zero and close to  $\pm 1$ , but not exactly equal. The matrix  $C$  has a *sparse* structure, but is not necessarily diagonal. This is because the eigenvectors on the subgraph correlate with those of the full graph at different indices  $i \neq j$  – unlike the full-to-full case, where the correspondence happens at  $i = j$ . A visual example of this correlation between eigenvectors is shown in the inset figure of Section 4.2 in the main paper.
- **(iii) Non-isomorphic subgraphs (this paper).** In case of subgraph rewiring, we still observe a correspondence between the eigenvectors of the full graph and those of the subgraph. However, the sparsity pattern of  $C$  tends to densify as the topological modifications increase.

As we discuss in the following and throughout the main paper, the presence of a structure in  $C$  for the cases (ii) and (iii) has not been observed before to our knowledge. This fact can find practical use in several applications; for example, by defining a regularizer that promotes a sparse or quasi-diagonal structure in  $C$  within graph learning pipelines, where the map  $C$  may be unknown and must be predicted.

### A.3 Comparison with smooth surfaces

In the case of smooth surfaces, it has been shown [43] that the sparsity pattern of matrix  $C$  can be well approximated by a simple formula. Given a surface  $\mathcal{M}$  and an isometric part  $\mathcal{N}$ , the matrix  $C$  is approximately diagonal, with diagonal angle  $\alpha$  proportional to the ratio of surface areas:

$$\alpha \sim \frac{\text{Area}(\mathcal{N})}{\text{Area}(\mathcal{M})}. \quad (4)$$

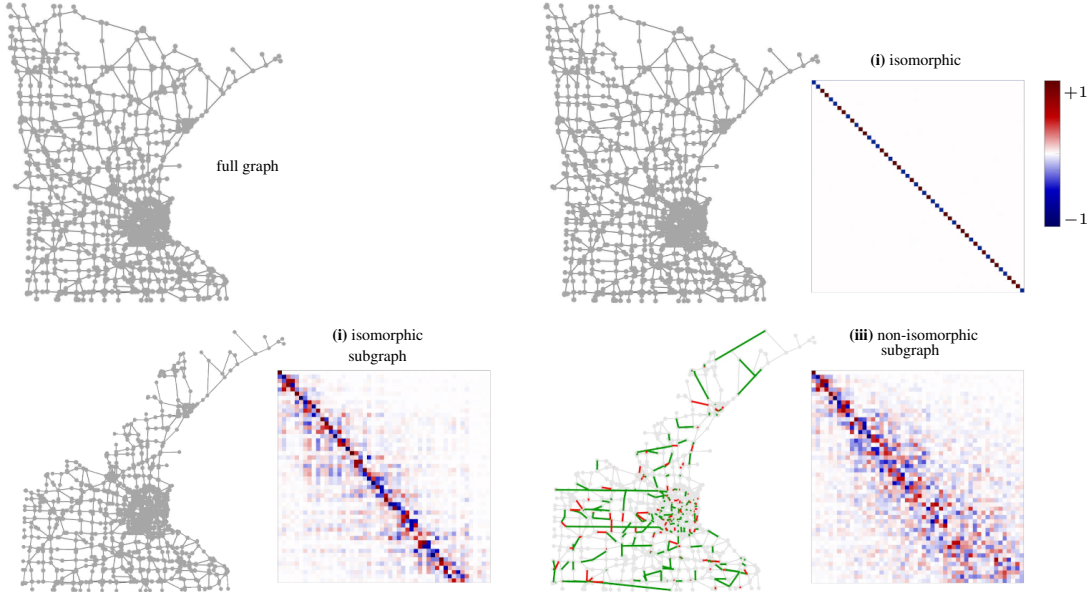


Figure 5: Functional maps of size  $50 \times 50$  between a full graph (depicted on the top left) and three different graphs, respectively: an isomorphic graph (top right), an isomorphic subgraph containing 80% of the original nodes (bottom left), and a *non*-isomorphic subgraph obtained by randomly rewiring the former (bottom right). The green edges are novel and randomly added (10% of the total), the red edges are randomly removed (10% of the total). The functional map still maintains a visible structure despite the significant changes of connectivity that span several hops.

As a special case, full-to-full isometric shape matching yields a diagonal matrix  $C$ , since  $\text{Area}(\mathcal{N}) = \text{Area}(\mathcal{M})$ . This result comes directly from an application of Weyl’s asymptotic law for Laplacian eigenvalues of smooth manifolds [48], which relates the eigenvalue growth to the surface area of the manifold via the relation:

$$\lambda_\ell \sim \frac{(2\pi)^2}{\text{Area}(\mathcal{M})^{2/d}} \ell^{2/d}, \quad \ell \rightarrow \infty \quad (5)$$

where  $d$  is the dimension of the manifold ( $d = 2$  for surfaces). We refer to [43, Eq. 9] for additional details pertaining surfaces.

However, Weyl’s law (Equation 5) does *not* hold for graphs, since there is not a well-defined notion of “area” of a graph. In fact, when we work with graphs and subgraphs, we observe that matrix  $C$  does not necessarily follow a diagonal pattern. More general sparse structures are observed in the coefficients of  $C$ , but an explanation rooted in differential geometry is not readily available.

In Figure 6, we report additional examples with large abstract graphs undergoing partiality transformations, showing that clear patterns appear rather consistently across different datasets.

Based on these observations, we believe there is an intriguing theoretical gap between what has been observed in the case of smooth manifolds, and what we report for graphs in this paper. In the former case, a geometric explanation has been proposed in the literature. In the latter case, empirical evidence yields similar results, yet it seems to be a purely algebraic phenomenon that remains to be addressed.

#### A.4 Number of eigenvectors

Given two graphs  $G_1$  and  $G_2$  with  $m$  and  $n$  nodes respectively, the node-to-node map  $S$  has size  $n \times m$ , thus scaling quadratically with the number of nodes.

By contrast, matrix  $C$  as defined in Equation 3 has dimensions that only depend on the number of Laplacian eigenvectors encoded in the matrices  $\Phi, \Psi$ . If one chooses the first  $k_1 \ll m$  Laplacian eigenvectors for  $G_1$  and the first  $k_2 \ll n$  Laplacian eigenvectors for  $G_2$ , the size of  $C$  is  $k_2 \times k_1$ . Observe that  $C$  is rectangular in general, but can be made square by choosing  $k_1 = k_2$  if so desired.

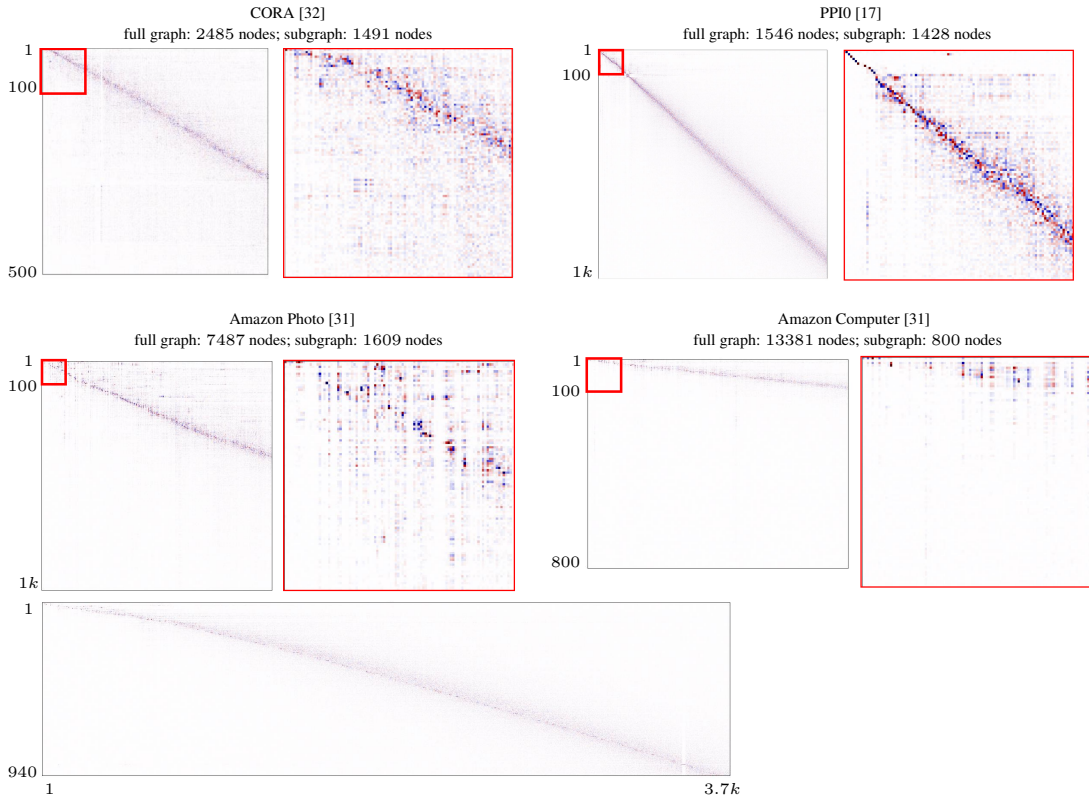


Figure 6: Functional maps computed over abstract graphs from 4 different datasets (CORA [32], PPI0 [17], Amazon Photo [31] and Amazon Computer [31]), showing a clear pattern in all cases. For each dataset, we compute the functional map  $C$  between the complete graph and a subgraph; the subgraph is obtained according to a semantic criterion depending on the dataset, e.g., for Amazon Photo, by considering the subgraph of nodes belonging to the same product category. For each functional map matrix  $C$ , we also show a zoom-in (framed in red). All the matrices are sparse, and have a clean structure that in some cases approximates a slanted diagonal. The wide matrix on the bottom is computed on Amazon Photo (using a different subgraph than the one used in the example above it), and shows that the sparse behavior is maintained throughout the entire spectrum.

As a general guideline, in this paper we typically use  $k = 20 \sim 50$  for a graph with 1000 nodes, leading to an especially compact representation  $C$ . Experiments under different choices of the number of eigenvectors  $k$  are shown in Figure 7 and Table 4.

## A.5 Regularizing behavior

Using  $k \ll n$  eigenvectors in the construction of  $C$  has a regularizing effect on the map, akin to a low-pass filtering of the correspondence.

In particular, when we use *all* the eigenvectors  $\Phi$  and  $\Psi$  to construct  $C$ , Equation 3 corresponds to an orthogonal change of basis; therefore, the representations  $S$  and  $C$  are equivalent and have the same dimensions. Truncating the bases to the first  $k_1$  and  $k_2$  eigenvectors, as described in Section A.4, yields a low-rank approximation  $C \approx S$ . In signal processing terms, we see the matrix  $C$  as a *band-limited* representation of the node-to-node correspondence  $S$ .

The regularizing effect is desirable in many cases, but is traded off for a loss in accuracy if a precise node-to-node correspondence is desired. On the one hand, if the map  $C$  is used to transfer a smooth signal (e.g. node-wise features like spectral positional encodings or carrying semantic information depending on the data), then the loss in accuracy is negligible, since Laplacian eigenvectors are optimal for representing smooth signals [1]; on the other hand, transferring non-smooth signals via a small  $C$  has the effect of filtering out the high frequencies. If high frequencies are desired, it is often sufficient to just increase the values of  $k_1, k_2$ , leading to a bigger matrix  $C$ .

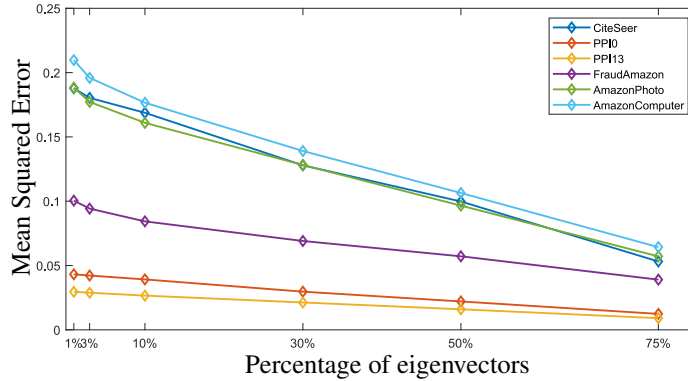
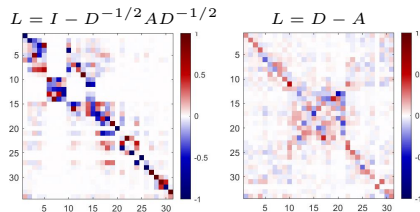


Figure 7: Normalized Mean Squared Error (MSE) obtained by transferring node features, using a functional map with increasing number of eigenfunctions (expressed as a percentage).

## A.6 Choice of Laplace operator

Our choice of the normalized graph Laplacian is mainly driven by the observation that alternative operators (such as the Laplacian  $L = D - A$ ) tend to exhibit worse preservation of their eigenspaces under partiality. This is manifested in a  $C$  matrix that is less sharp and that tends to be less sparse, as shown in the inset figure on the Karate dataset.



In the special case where the graph is constructed on top of a point cloud sampled from a (possibly high-dimensional) manifold  $\mathcal{M}$ , it has been shown that the eigenvectors of the normalized graph Laplacian converge to the eigenfunctions of the Laplace-Beltrami operator on  $\mathcal{M}$  [2]. However, as discussed in Section A.3, our case is more general. We consider generic abstract graphs without an explicit underlying manifold, i.e. we do not construct our graphs from input point clouds. Further, in [2] it is assumed that  $\mathcal{M}$  is a compact infinitely differentiable Riemannian submanifold of  $\mathbb{R}^d$  *without* boundary, meaning that partiality transformations, which are the main focus of this paper, are not considered.

## B Additional experiments

### B.1 Partiality percentage

The aim of this experiment is to study how much the performance of the functional representation for a correspondence task degrades with different levels and types of partiality.

In Table 3, we perform an experiment similar to the one in section 5.3 of the main paper and test how the MAP of the correspondence changes when we consider subgraphs of different dimensions. In particular, we test 2 partialities: patch and holes. The former is obtained by expanding a neighborhood from a given random node until a certain number of nodes is reached. The latter is obtained by removing random nodes with their immediate neighborhood. The main difference is in the sparsity of the two partialities. The first keep a cluster of nodes without changing the inner connectivity of the graph; the latter is sparser in the sense that it removes the path between nodes of the graph, changing the whole connectivity of the graph.

### B.2 Number of eigenvectors

In Table 4, we report the correspondence accuracy obtained from ground-truth functional maps ( $GT$  in the main paper) under increasing percentage of eigenvectors.



Table 3: MAP(%) of the correspondence on different datasets at decreasing size of the sub graph (expressed as percentages, decreasing from 90% to 50%) with two type of partiality: patch (first table) and holes (second table). The correspondences are obtained from ground-truth functional maps.

patch	90%	80%	70%	60%	50%
Minnesota	95.82 ± 1.84	<b>96.0</b> ± 1.98	94.47 ± 1.90	94.00 ± 1.60	94.12 ± 1.27
CORA [32]	<b>82.67</b> ± 2.40	74.45 ± 2.27	67.20 ± 2.56	65.00 ± 3.10	60.03 ± 2.45
Citeseer [32]	<b>83.12</b> ± 1.88	77.68 ± 3.48	71.33 ± 4.48	68.50 ± 3.13	65.41 ± 5.21

holes	90%	80%	70%	60%	50%
Minnesota	<b>68.19</b> ± 1.91	50.36 ± 4.11	46.28 ± 3.5	51.70 ± 3.00	53.80 ± 3.30
CORA [32]	<b>70.0</b> ± 3.58	55.52 ± 4.16	45.59 ± 2.67	41.87 ± 2.30	38.08 ± 2.90
Citeseer [32]	<b>74.80</b> ± 2.83	62.4 ± 2.70	54.97 ± 2.47	51.07 ± 3.21	48.87 ± 2.80

Table 4: MAP(%) of the correspondence on different datasets at increasing number of eigenvectors (expressed as percentages, growing from 1% to 75%). The correspondences are obtained from ground-truth functional maps.

	Partiality	1%	3%	5%	10%	30%	50%	75%
Cat [10]		86.97 ± 4.92	97.65 ± 0.93	99.23 ± 0.41	99.98 ± 0	<b>100</b> ± 0	<b>100</b> ± 0	<b>100</b> ± 0
Minnesota	patch	70.77 ± 4.54	90.05 ± 1.97	94.42 ± 1.22	97.78 ± 0.46	99.62 ± 0.1	99.98 ± 0	<b>100</b> ± 0
CORA [32]		49 ± 4.51	68.41 ± 3.5	76.22 ± 2.67	84.28 ± 0.96	93.15 ± 0.56	99 ± 0.18	<b>99.54</b> ± 0.12
CORA [32]	class	71.35 ± 9.24	86.87 ± 3.71	90.18 ± 2.65	93.57 ± 1.16	95.96 ± 0.33	99.08 ± 0	<b>99.5</b> ± 0
Douban [49]	online-offline	1.6	4.23	8.3	19.91	64.46	96.33	<b>98.97</b>

### B.3 Rewiring

In the main paper and in Figure 8, we highlight how the functional map degrades when we apply a sequence of local rewiring operations. Here we consider a much stronger variation, namely, a *global* rewiring where we do not limit the topological perturbation to a local neighborhood. The results are reported in Figure 9.

## C Dataset and implementation details

In this section we report additional details about the experimental setup used in the main manuscript.

### C.1 Datasets

In Table 5 we sum up the main statistics across all the datasets and benchmarks used in our experiments. In addition to number of nodes, number of edges, graph diameter and average node degree, in the table we also report the application domain of each dataset, the task where they are used, the type and number of node-wise features (where used). Since PPI and QM9 are a collection of graphs, we used only a few of them. In particular, from the PPI dataset we used the first and fourteenth (specified with 0 and 13 in the experiments) graphs.

Table 5: Summary of statistics about the datasets used in our experiments.

Dataset	Nodes	Edges	Diameter	Average degree	Domain	Task	Features	Number of features
Cat [10]	10000	19940	86	5.99	Geometry processing	Shape matching	-	-
Minnesota	2635	3298	98	2.5	Roadmap	-	-	-
Karate [51]	34	78	5	4.59	Social networks	Node classification	-	-
QM9 [22]	29	47	6	3.24	Chemistry	Graph regression	-	-
Cora [32]	2485	5069	19	4.08	Citation networks	Node classification	-	-
Douban [49]	3906	8164	13	4.18	Social networks	Network alignment	-	-
Citeseer [16]	2120	3731	28	3.50	Citation networks	Node classification	Bag-of-Words	3703
Pubmed [44]	19717	44327	28	0.00	Citation networks	Node classification	Bag-of-Words	500
PPI [17] 0	1546	17699	8	21.90	Chemistry	Graph regression	Gene attributes	50
PPI [17] 13	3480	56857	8	31.68	Chemistry	Graph regression	Gene attributes	50
FraudAmazon [53]	11944	4417576	4	739.71	Product reviews	Fraud detection	Bag-of-Words	25
Amazon Photo [31]	7487	119044	11	31.80	Co-purchase	Node classification	Bag-of-Words	745
Amazon Computer [31]	13381	245778	10	36.74	Co-purchase	Node classification	Bag-of-Words	767

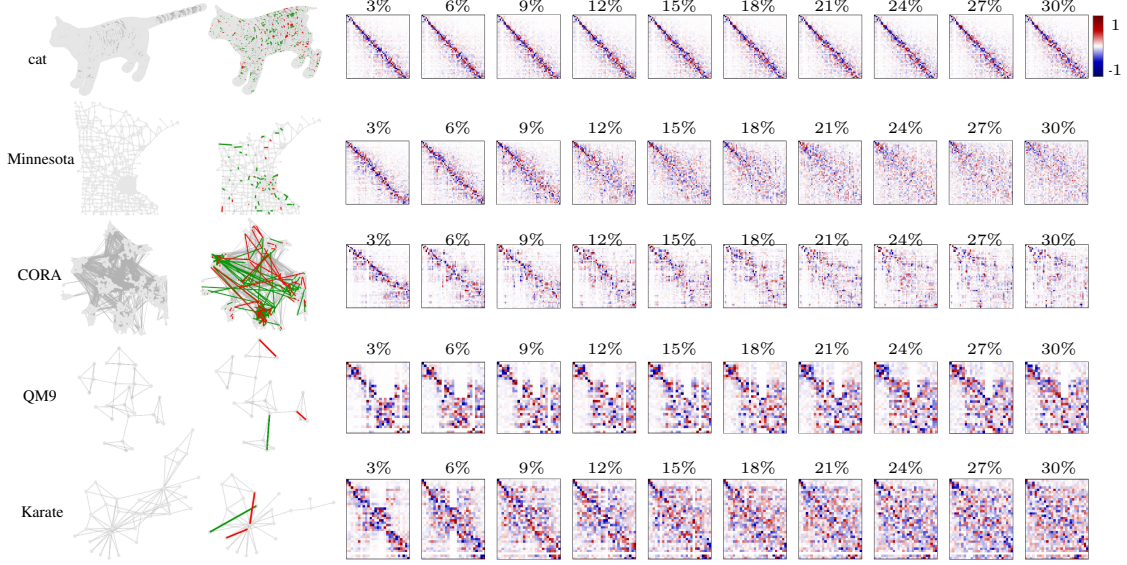


Figure 8: Robustness of the map to the simultaneous action of partiality and rewiring of the subgraph. The rewiring operations are increasingly **stronger**, with increments of 3% of the total number of edges (starting from 3% and reaching 30%). Differently from the figure in the main paper, the plotted matrices represent the functional map after the topological perturbations, showing the effect of rewiring on the functional map structure.

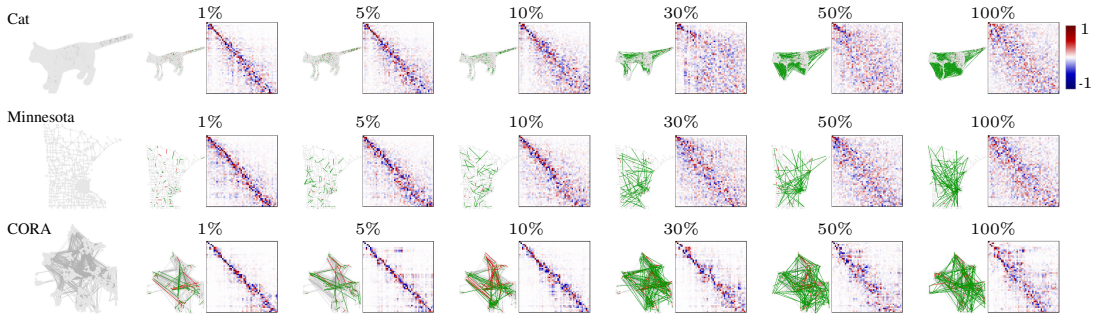


Figure 9: Robustness of the map to the simultaneous action of partiality and rewiring of the subgraph. The rewiring operations are increasingly **wider**, involving nodes and edges farther apart. The left column shows the full graph, while the pairs composed by a graph and a matrix show the rewiring operation and the resulting functional map, starting with a rewiring involving just nodes within 1% of the graph diameter (left) up to the full graph diameter (right).

## C.2 Implementation of node-to-node map inference

As stated in the main manuscript, to test the effectiveness of the spectral representation when seeking a node-to-node correspondence matrix, we adopt the off-the-shelf partial functional maps algorithm ( $FM_W$ ) [43] and then refine the correspondence with ZoomOut [34] ( $FM_W + ZM$ ). These algorithms are not specifically designed for graph matching, but can work with generic spectral representations, which is one of their main benefits.

We implemented the  $FM_W$  optimization in MATLAB through the manopt package [4]. We considered a minimization problem with the form:

$$C = \arg \min_{C \in \mathbb{R}^{k \times k}} \|CA - B\|_{2,1} + \mathcal{R}(C), \quad (6)$$

where  $A$  and  $B$  are the coefficients in the Laplacian basis for a set of corresponding probe functions, while  $\mathcal{R}(C)$  is some additional regularizer. As probe functions we computed smooth  $\delta$  functions for the given set of landmark matches. For all the methods that accepted nodes features (FINAL,

REGAL, GRASP) as input, we used the same functions as nodes features.  $\mathcal{R}(C)$  fosters additional structure to  $C$  and is defined as:

$$\mathcal{R}(C) = \mu_1 \|C \odot W\|_2^2 + \mu_2 \sum_{\ell \neq h} (C^\top C)_{\ell,h}^2 + \mu_3 \sum_{\ell} ((C^\top C)_{\ell,\ell} - d_\ell)^2, \quad (7)$$

where each term has its weight  $\mu_1$ ,  $\mu_2$  and  $\mu_3$ .  $W$  is a mask matrix that acts through element-wise multiplication  $\odot$  and encodes the relation between the eigenvalues of the two shapes, which approximates the slanted-diagonal structure of  $C$  induced by the partiality. In particular, we computed  $W$  with the complex resolvent method proposed in [42]. The term weighted by  $\mu_2$  promotes orthogonality of the map by penalizing the off-diagonal entries of  $C^\top C$ . Finally  $d_\ell \in \{0, 1\} \forall \ell$ ; the entries equal to 1 represent which singular values of  $C$  are expected to be non-zero. A refinement, similar to the iterative closest point algorithm [3] in the space of the coefficients, is then applied to the matrix  $C$ . As a final step, the spectral refinement approach of ZoomOut [34] is applied to the computed  $C$ . Given a map of size  $50 \times 50$  as input, we apply ZoomOut to its  $37 \times 37$  sub-matrix and get back a refined matrix  $C_{ZM}$  of size  $50 \times 50$ .

The ground-truth functional map ( $GT$ ) is obtained through Equation 3 where  $S$  is the ground-truth correspondence matrix.

All the methods we compared to in section 5.3 of the main paper were taken from the public benchmark [46]. To run the experiments, we used the standard parameters suggested in their code. As node features, we used the same probe functions defined from the landmarks as in  $FM_W$ . PALE was trained on the ground-truth correspondences given by the 50 landmarks.

### C.3 Computational time

In Table 6, we report the optimization time needed to compute the correspondences of Table 2 from the main paper. For functional map-based matching algorithms ( $FM_W$ ,  $FM_W + ZM$ ) we did not consider the computation of the eigenvectors since it is an offline cost as eigenvectors can be pre-computed once and re-used. For  $FM_W + ZM$ , we only report the computational time of ZoomOut refinement starting from an input functional map. All the experiments were performed on a Intel(R) Core(TM) i7-9700K CPU @ 3.60GHz.

Table 6: Comparison of the computational time (in seconds) needed by different methods to compute a node-to-node correspondence, across several datasets. Spectral based methods (last two columns) are the most efficient.

	Partiality	IsoRank	FINAL	REGAL	PALE	GRASP	$FM_W$	$FM_W + ZM$
Cat[10]	patch	$270.44 \pm 9.84$	$156.49 \pm 2.73$	$36.78 \pm 0.86$	$3586.4 \pm 109.5$	$1057.7 \pm 100.59$	<b>20.73</b> $\pm 1.67$	<b>5.45</b> $\pm 0.28$
Minnesota		$32.18 \pm 3.94$	$10.21 \pm 0.15$	$7.08 \pm 0.07$	$145.72 \pm 9.14$	$648.43 \pm 267.5$	<b>2.83</b> $\pm 0.66$	<b>0.33</b> $\pm 0.03$
Cora[32]	class	$31.54 \pm 3.1$	$10.48 \pm 0.55$	$7.33 \pm 0.15$	$211.99 \pm 1.87$	$198.22 \pm 148.3$	<b>2.89</b> $\pm 0.42$	<b>0.39</b> $\pm 0.4$
Cora[32]		$14.92 \pm 2.4$	$51.61 \pm 10.2$	$10.92 \pm 0.9$	$434.13 \pm 35.6$	$118.61 \pm 72$	<b>1.96</b> $\pm 0.1$	<b>0.38</b> $\pm 0.02$
Douban[49]	online-offline	11.54	27.07	10.41	337.56	16.32	<b>4.43</b>	<b>0.03</b>